Int. J. Electrochem. Sci., 17 **(2022)** Article Number: 220140, doi: 10.20964/2022.01.01

International Journal of
ELECTROCHEMICAL
SCIENCE
www.electrochemsci.org

Study of Crevice Corrosion Behavior and Cathodic Protection of Carbon Steel Reinforcement in Concrete

Jiuquan Chen, Lingfeng Ji[*], *Jinwei Song*

Hebei Construction Material Vocational and Technical College, Qinhuangdao 066004, China
[*]E-mail: teacher_ji1234@163.com

Received: 3 September 2021 / *Accepted:* 19 October 2021 / *Published:* 6 December 2021

Chloride ion ingress is one of the critical factors causing concrete failure in structures. Cathodic protection is widely used in concrete for corrosion protection as it promotes interface alkalization and removes chloride ions. However, some positions are in an over-protected state due to cracks in concrete, especially at the concrete-reinforcement interface. Therefore, based on immersion and electrochemical experiments, this paper evaluates the optimal cathodic protection potential of reinforcement under different temperatures through corrosion rate, morphology, and electrochemical parameters, and the electrochemical characteristics of the metal at the opening under the condition of optimal cathodic protection potential. The results showed that with the increase of cathodic protection level, HRB335 steel exhibited a general corrosion state at 20℃. However, the corrosion state changed from pitting to comprehensive corrosion at 50℃ and 80℃, and the oxygen diffusion process controlled the optimal cathodic protection potential. Considering the corrosion rate, morphology, and electrochemical reaction control process, the optimal cathodic protection potential was -1.0 V and -1.1 V at 50℃ and 80℃, respectively. Meanwhile, when the HRB335 steel in the deepest crevice reached the optimal cathodic protection potential, the metal in the opening may be in an over-protected state, and a hydrogen evolution reaction occurred. The higher the temperature, the higher was the metal potential and the more pronounced was the hydrogen evolution reaction.

Keywords: Reinforced concrete; Corrosion potential; Cathodic protection; Concrete deterioration

1. INTRODUCTION

The reinforced concrete structure is one of the most critical structural forms in infrastructure construction. With the completion of many reinforced concrete structures, various problems affecting the use, function, and safety of the structure appear in the design life, attracting more and more attention by the researchers [1]. It has been confirmed that concrete durability damage caused by chloride corrosion is one of the primary factors in concrete deterioration and failure.

After hundreds of years of research and development, cathodic protection (CP) has been widely accepted in the anti-corrosion industry. It has been proven by corrosion scientists to be the best way to prevent chloride ions from penetrating reinforced concrete structures [2]. The British Standards Organization points out that cathodic protection is the only way to protect the reinforcement from chloride ions in concrete structures. The American Concrete Institute also emphasizes that only cathodic protection is the most effective way of preventing the continued corrosion of existing concrete structures.

However, for the reinforced concrete structures, a small part of the reinforcement is difficult to be protected as there are many cracks in the concrete, particularly at the concrete-reinforcement interface. If all the reinforcements are required to be protected, it will need much more CP current, and even cause hydrogen evolution reaction in many areas of the reinforcements with overprotection, which may also reduce the bond at the concrete-reinforcement interface [3-5]. Due to the CP current, a large amount of OH^- will be generated on the surface of the protected reinforcements, resulting in an alkaline environment to promote the reinforcements to form a protective film. At the same time, because the CP current has a forced driving effect, Cl^- in the concrete near the protected reinforcement is transferred from the cathode to the anode, which significantly reduces the Cl^- content on the surface of the protected reinforcement, thus playing a protective role for the reinforcement [6].

Compared with coated reinforcement, corrosion inhibitor, and other technologies, CP technology has the advantages of no pre-treatment, easy maintenance, longer service life, and low cost [7]. However, the setting of cathodic protection potential is affected by the ambient temperature. Therefore it is necessary to analyze the optimal cathodic protection potential. On the other hand, the crevice structure of concrete has a certain shielding effect on CP. Therefore, in this paper, the optimal cathodic protection potential under different temperatures through electrochemical experiments and immersion experiments have been studied, and the electrochemical reaction process of the metal in the opening when the metal in the deepest crevice reached the optimal cathodic protection potential has been revealed.

2. MATERIALS AND EXPERIMENTAL METHODS

2.1 Immersion test

The properties of HRB335 steel used as the metal material for the test. Different CP potentials (-0.85 – -1.2 V) were applied through DC (direct current) power source, and different temperatures (20℃, 50℃, and 80℃) were obtained through water bath heating and constant temperature-humidity chamber. Three parallel samples for immersion for five days were set up for each group of experiments. After the immersion experiment, the corrosion products were removed by the standard cleaning fluid, and the corresponding mass loss was calculated. Meanwhile, the corrosion morphology and maximum pitting depth were observed by Zeiss 3D scanning microscope, in which the general corrosion rate (Eq.1) and pitting corrosion rate (Eq.2) could be determined under different temperatures (20℃, 50℃,

and 80℃) and CP potentials (-0.85 V, -1.0 V and -1.2 V). The experimental setup is shown in Figure 1(1).

$$v_1 = 87600 \times \frac{\Delta G}{S \times t \times \rho} \quad (1)$$

Where, v_1 was total corrosion rate in mm/a, $\triangle G$ was the weight loss of HRB355 steel in g, S was surface area of 1 cm^2, t was experimental time in h and ρ was HRB355 density of 7.85 g/cm^3.

$$v_2 = 87600 \times \frac{H_{max}}{t} \quad (2)$$

Where, v_2 was pit corrosion rate in mm/a, H_{max} was the max pit depth obtained by Zeiss Microscope in mm and t was experimental time in h.

2.2 Polarization curve test

The polarization curve was tested using a three-electrode system, as shown in Figure 1(2), in which the reference potential (RE) was saturated calomel electrode (SCE), the auxiliary electrode (AE) was platinum electrode (Pt), and the working electrode (WE) was HRB335 steel (size 10×10×2 mm^3).

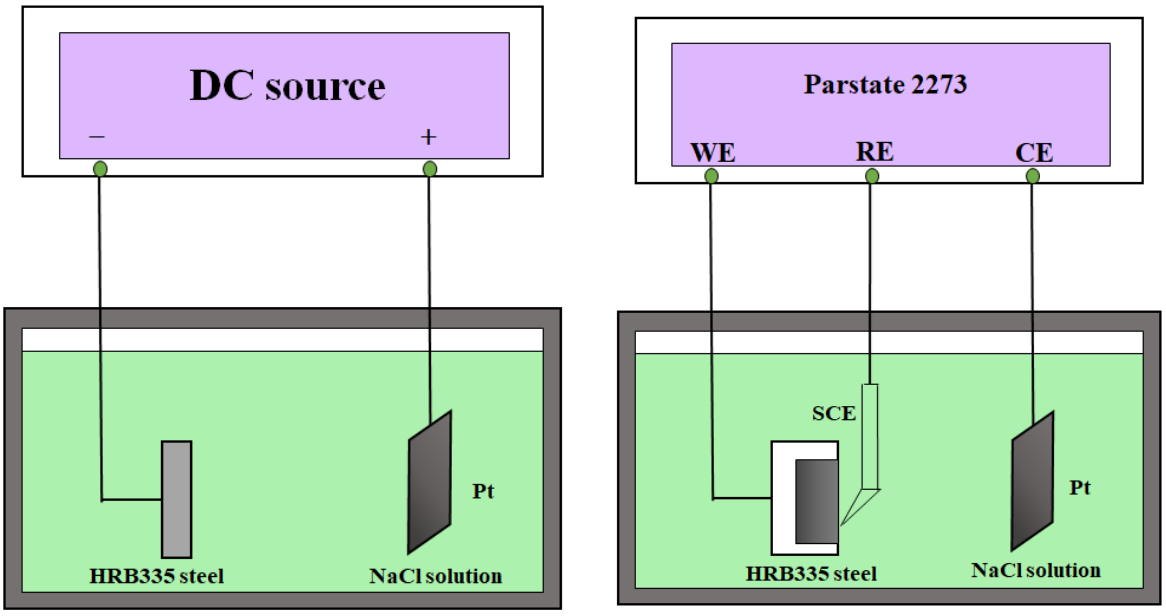

(1) Immersion experiment device (2) Electrochemical test device

Figure 1. Experiment diagram (immersion test and electrochemical test) of HRB335 steel in 3 wt % NaCl solution under different temperatures (t = 20℃, 50℃ and 80℃) and CP potential (CP = -0.85 V, -1.0 V and -1.2 V): (1) Immersion experiment device, and (2) Electrochemical test device

NaCl solution with a mass fraction of 3.5% was used as the experimental solution. The experiments were conducted at the temperatures of 20℃, 50℃, and 80℃. The metal samples for electrochemical testing were cleaned with acetone, deionized water, and alcohol successively. After

drying, the copper wires were welded and then encapsulated by epoxy resin, with a working area of 10×10 mm^2. Before the experiment, the working surface of the test sample was polished. The reference electrode was connected through a Luggin capillary. The distance between the WE and the Luggin capillary tip was less than 2 mm; therefore, the IR drop between the reference electrode and the WE could be ignored.

The electrochemical workstation used Princeton PARSTST 2273. When the open circuit potential (OCP) of the WE fluctuated within 300 s at ±10 mV, the polarization curve was tested. The scanning potential range was ±250 mV (vs.OCP), and the scanning rate was 0.01667 mV/s. PowerSuite software of the system was used for the data analyses.

2.3 Optimal CP potential

A wedge crevice experimental device was used to simulate the crack structure in concrete (Figure 2). The cover plates were made of transparent PE (Poly Ethylene) material, and the gap angle was 1°(with a gap width of up to 0.3 mm) [8]. A test sample was arranged at the opening, and five test samples were arranged at 3-15 cm away from the opening, termed as 0 - 1#，3 cm - 2#，6 cm - 3#，9 cm - 4#，12 cm - 5# and 15 cm - 6#, respectively. The sample material and the solution were the same as described earlier in Section 2.2. According to the protocol during the electrochemical tests, a reference electrode and an auxiliary electrode were set at each test piece location to investigate the electrochemical impedance spectrum (EIS).

The applied DC source realized the cathodic protection of the experimental device, and the auxiliary anode was the Pt electrode. Taking the potential of the 6# sample as the reference, the different optimal CP potential under different temperatures was achieved by adjusting the variable resistance and DC power output. The change of potentials and EIS curves of 1# sample were monitored.

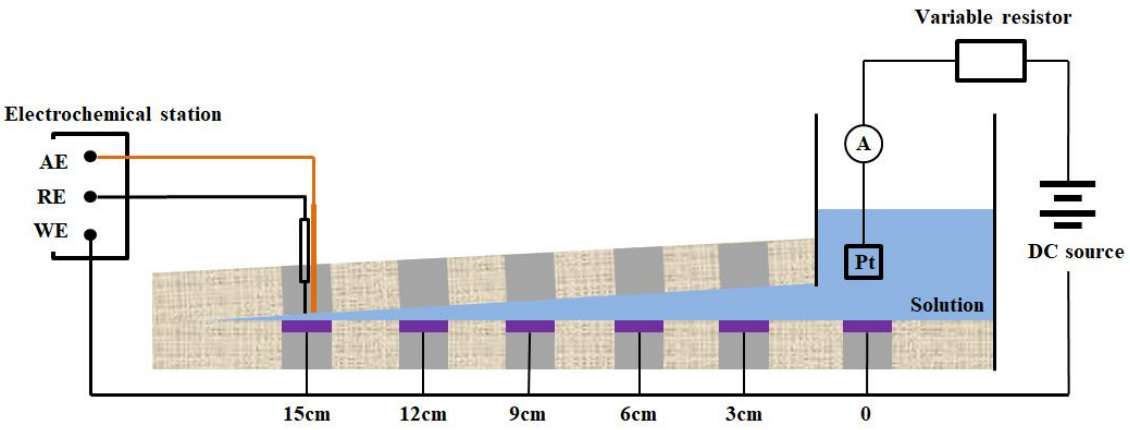

Figure 2. Wedge-shaped crevice device for simulating concrete crevice to carry out immersion test and electrochemical test of HRB335 steel in 3 wt % NaCl solution under different temperatures (t = 20℃, 50℃ and 80℃) and CP potential (CP = -0.85 V, -1.0 V and -1.2 V)

3. RESULT AND DISCUSSION

3.1 Effectiveness analysis of cathodic protection potential under different temperatures

3.1.1 Analysis on corrosion rate

Figure 3 shows the general corrosion rate and pitting corrosion rate of HRB335 steel under varying experimental temperatures and CP potentials. Nowadays, it is considered that when the corrosion rate of metal is less than 0.076 mm/a, the corrosion level of metal is in an acceptable range [9-11]. It can be seen from the test results in Figure 3, under the experimental temperature of 20℃, the general corrosion rate and pitting rate of HRB335 steel change slightly, in which the average was respectively 0.034 mm/s and 0.016 mm/a. Both the general corrosion rate and pitting corrosion rate were observed less than the upper limit of 0.076 mm/a, indicating that at the experimental temperature of 20℃, CP could effectively protect HRB335 steel. By comparing the general corrosion rate and pitting corrosion rate, it can be seen that HRB335 steel was in the general corrosion state under effective CP. At 50℃ and 80℃, the general corrosion rate and pitting rate of HRB335 steel all decreased with the increase of CP level. At a small CP level (-0.85 V), the general corrosion rate and pitting corrosion rate of HRB335 steel at 50℃ were 0.086 mm/a and 0.105 mm/a, respectively. At 80℃, the general corrosion rate and pitting rate of HRB335 steel were 0.130 mm/a and 0.323 mm/a, respectively. At this time, the general corrosion rate and pitting corrosion rate of HRB335 steel were higher than 0.076 mm/a, and the CP did not provide complete protection. Also, HRB335 steel was in a pitting corrosion state, and the higher the temperature, the more obvious pitting characteristics [12,13].

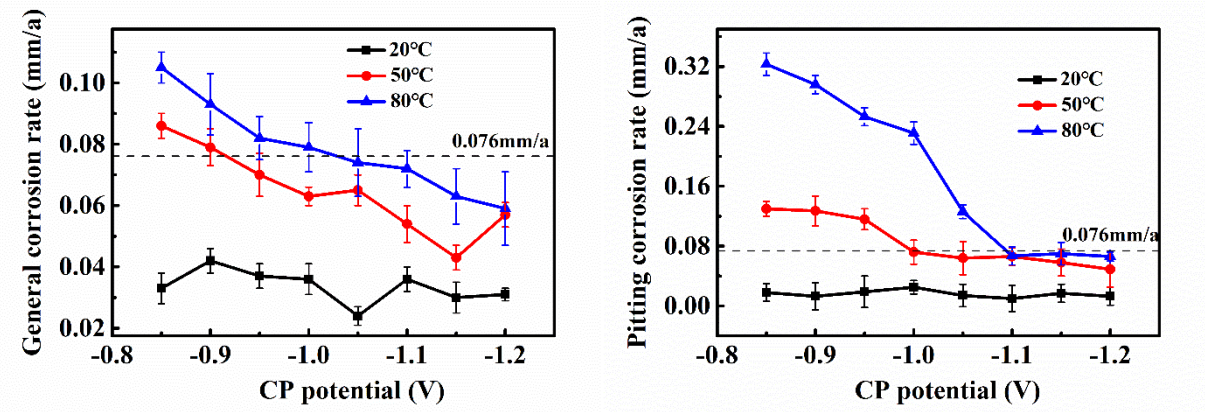

Figure 3. The general and pitting corrosion rate of HRB335 steel immersing in 3 wt % NaCl solution for 5 days using wedge-shaped crevice device under different temperatures (t = 20℃, 50℃ and 80℃) and CP potential (CP = -0.85 – -1.2 V, including eight CP values at 0.5 V intervals)

3.1.2 Analysis on corrosion morphology

Figure 4 shows the corrosion image characteristics of HRB335 steel under different experimental temperatures (20℃, 50℃, and 80℃) and CP potentials (-0.85 V, -1.0 V, and -1.2 V). It can be seen that at 20℃, the metal surface of HRB335 steel under different CP potential was in a

general corrosion state. With the increase of CP level, the surface corrosion morphology became more uniform. From the results of the general rate, it can be seen that the corrosion degree changed mildly, but the surface was relatively uniform. At 50℃, the surface of HRB335 steel showed an obvious pitting state at CP = -0.85 V. When it was increased to -1.0 V, the pitting characteristics gradually disappeared [14]. However, the metal surface still showed a prominent corrosion area. When the negative retention potential was -1.2 V, the corrosion state changed to general corrosion. At 80℃, the pitting characteristics at -0.85 V were stronger than those at 50℃. When the CP potential was -1.0 V, the pitting characteristics still existed but weakened significantly [15]. When it increased to -1.2V, the pitting characteristics changed into general corrosion, but the corrosion degree was greater than that observed at 20℃ and 50℃. Therefore, it can be determined as the optimal cathodic potential when the pitting state changes to the general corrosion [16].

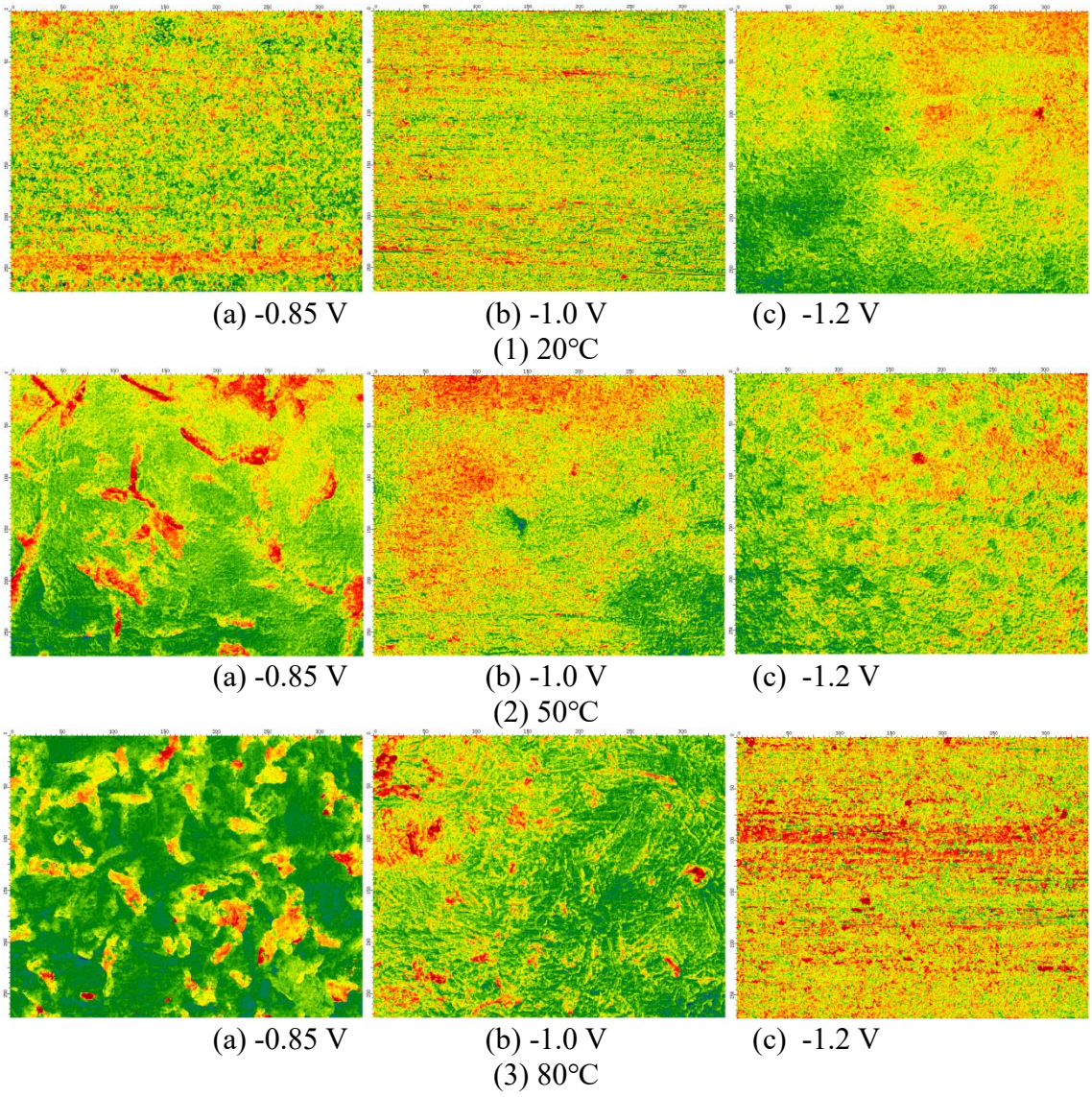

Figure 4. The corrosion morphology of HRB335 steel immersing in 3 wt % NaCl solution for 5 days using wedge-shaped crevice device under different temperatures (t = 20℃, 50℃ and 80℃) and CP potential (CP = -0.85 V, -1.0 V and -1.2 V): (1) t = 20℃, (2) t = 50℃, and (3) t = 80℃; (a) CP = -0.85 V, (b) CP = -1.0 V, and (c) CP = -1.2 V

3.2 Analysis of the optimal cathodic potential of HRB335 steel under different temperatures

Figure 5 shows the polarization curves of HRB335 steel under different temperatures. The fitting data (shown in Table 1 and Table 2) showed the potential ranges at different stages of the cathode reaction process. At 20℃, 50℃, and 80℃, the corrosion potential of HRB335 steel was -0.798 V, -0.843 V, and -0.873 V, respectively [17]. The corrosion potential of HRB335 steel was negatively shifted, meaning that the corrosion tendency of the metal increased. Meanwhile, when the temperature increased from 20℃ to 50℃, the corrosion current density increased by 1.8 times. In contrast, when the temperature increased from 50℃ to 80℃, the corrosion current density increased by 4.7 times, indicating that the temperature increase accelerated the metal corrosion, and the current density required for external CP increased at this time.

Under different temperatures, the Tafel region in anodic polarization curves of HRB335 steel was an activation control. The shape of the anode polarization curve had no noticeable change, and the anode Tafel constant was equal, indicating that the corrosion process of the metal matrix had not changed with the changing temperatures. In the cathode region (Stage A) of the polarization curve, the over-potential was 102 – 127 mV, under different temperatures in the active corrosion section, and the corresponding polarization current density values were 8.18 $\mu A/m^2$, 16.9 $\mu A/m^2$, and 580 $\mu A/m^2$, respectively [18]. The current density increased sharply, indicating that the higher was the temperature, the lower was the corresponding linear resistance of the metal. As the cathodic over-potential further increased, the cathodic polarization curves under different temperatures entered the second stage (Stage B). In the limiting diffusion current density stage, the over-potential was 270 mV at 20℃, while it was all 50 mV at 50℃ and 80℃, which was far smaller than the over-potential at low temperature (20℃).

Considering the cathodic protection of HRB335 steel under different temperatures, the optimal protection potential of metal has been determined by several researchers through the anode Tafel extrapolation method according to the theory of electrochemical kinetics which had been well corroborated in engineering applications.

The optimal CP potentials under different temperatures were -0.859 V, -0.959 V, and -1.001 V, respectively, by extrapolation of Tafel curves. The current international general CP criterion considers that the corrosion rate of pipelines can be accepted when the outage potential of pipelines is between -0.85 – -1.2V (CSE, Saturated copper sulfate electrode). It can be seen that the optimal CP potential under different temperatures was well within the normal range of cathodic potential. It is suitable for the cathodic protection of metal at 20℃. However, when the temperature increased to 50℃, the optimal CP potential had shifted to -0.959 V or even more negative. The optimal CP potential in the existing criteria cannot met the requirements. According to the German standard DIN 30676-1983, the optimal CP potential of metal is -0.95 V (CSE) in an environment with a temperature greater than 60℃, which is similar to the results obtained in this study. Therefore, according to the results obtained in this study, at 20℃, the optimal CP potential was affected by activation control, while at 50℃ and 80℃, the optimal CP potential was were controlled by the oxygen diffusion process [19-21]. The optimal CP potential of HRB335 steel at high temperature was determined by combining the general corrosion rate and pitting corrosion rate. The optimal CP potential was -1.0 V at 50℃ and -1.1 V at 80℃, which

were both inside the range of the oxygen diffusion control stage combined with the polarization curve [22].

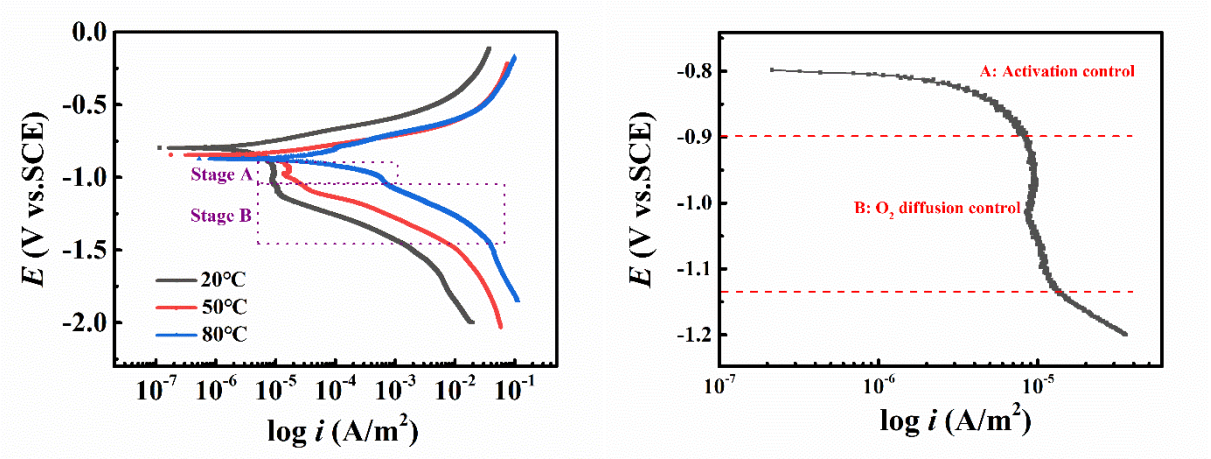

(1) Polarization curve (2) Cathodic curve at 20℃

Figure 5. Polarization curves of HRB335 steel in 3 wt % NaCl solution under different temperatures (t = 20℃, 50℃ and 80℃): (1) Polarization curve, and (2) Cathodic curve at 20℃

Table 1. The fitting results of polarization curves of HRB335 steel in 3 wt % NaCl solution under different temperatures (t = 20℃, 50℃ and 80℃)

Temperature / (℃)	E_{corr} / (V)	I_{corr} / (μA/cm^2)	β_a / (mV)	β_c / (mV)	Min CP / (V)
20	-0.798	3.86	38	40	-0.859
50	-0.843	6.98	40	48	-0.959
80	-0.873	32.71	39	59	-1.001

Table 2. The potential range of different stages on cathodic polarization curves of HRB335 steel in 3 wt % NaCl solution under different temperatures (t = 20℃, 50℃ and 80℃)

Stage / Temperature	A	B
20℃	-0.798~-0.90 V	-0.90~-1.17 V
50℃	-0.843~-0.95 V	-0.95~-1.00 V
80℃	-0.873~-1.00 V	-1.00~-1.05 V

3.3 EIS curves of 1# sample with optimal CP potential under different temperatures

The optimal CP potential for the 6# sample was set at 50℃ and 80℃, respectively. Due to the shielding effect of crevice structure on cathodic current, when the potential of the 6# sample stabilized, the potential of 1# sample was obtained to be -1.09 V (50℃) and -1.27 V (80℃), respectively. Related studies pointed out that hydrogen evolution reaction will occur when the potential of Fe-base metal is negative to -1.2 V in the near-neutral environment [23].

Figure 6 shows the variation of the EIS curves of HRB335 steel with time under different experimental temperatures. Under the research conditions set out in this study, it can be seen from

Figure 2 that the HRB335 steel was always in an activation corrosion state. According to the relevant theory of oxygen concentration battery for crevice corrosion [24,25], the 6# sample was the anode, and the 1# sample was the cathode. However, considering the possible corrosion of 1# sample, such as hydrogen evolution reaction and Bode diagram characteristics, the equivalent circuit was chosen as $R_s(Q(R_p(C_{dl}R_{ct})))$, in which R_s was the solution resistance, Q was the system capacitance, R_p was the film polarization resistance, C_{dl} was the double-layer capacitance, and R_{ct} was the charge transfer resistance. Table 3 shows the fitting parameters of EIS curves under different experimental temperatures.

As shown in Figure 6, under different CP potential conditions, the radius of the Nyquist diagrams arc gradually decreased with the increase of the experimental time, indicating that the corrosion resistance of the metal had weakened, which may be attributed to the intergranular corrosion and hydrogen evolution reaction of HRB335 steel at high temperature [26]. Further, the lower the cathodic protection level, the greater was the arc radius of capacitive reactance. It indicates that the corrosion resistance of HRB335 steel was lower with CP = -1.27 V. Compared to the Nyquist diagrams with CP = -1.09 V, the Nyquist diagrams with CP = -1.27 V showed incomplete capacitive characteristics, which was due to the hydrogen evolution reaction of metal at a higher CP potential level [27]. The corrosion products on metal surface were incomplete due to hydrogen adsorption and hydrogen diffusion. The phase angle curves with CP = -1.09 V showed an obvious peak value, while the phase angle curves of CP = -1.27 V showed two peak value characteristics. The maximum phase angle amplitude θm_{ax} decreased gradually with the experiment time. The maximum phase angle frequency $f_{\theta\text{-max}}$ changed to the low frequency representing the mass diffusion process, indicating that with the increase of the experiment time, the resistance of the corrosion product layer was reduced. The corrosion product film structure was gradually becoming loose to diffuse, therefore in log$f$-|Z| curves, mass diffusion impedance at 10^{-2} Hz decreased gradually with the increase of test time, indicating a higher corrosion rate [28].

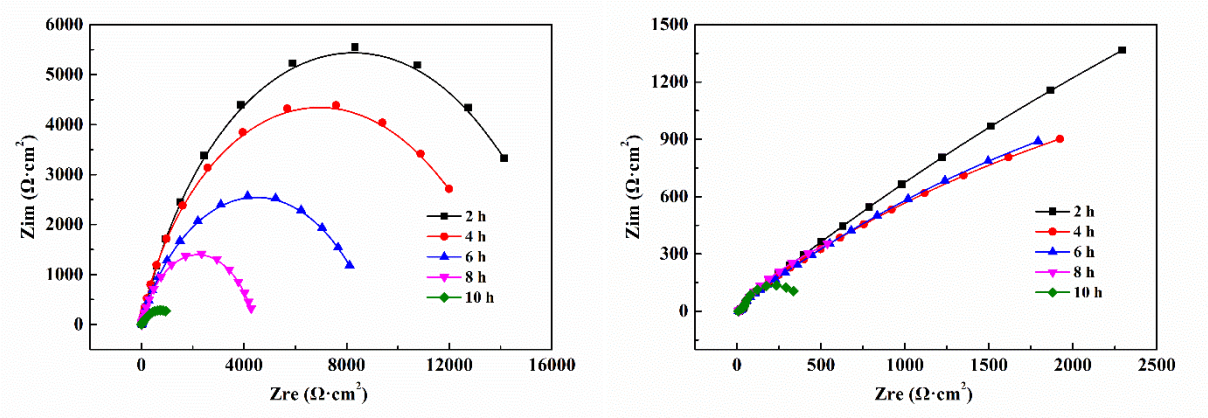

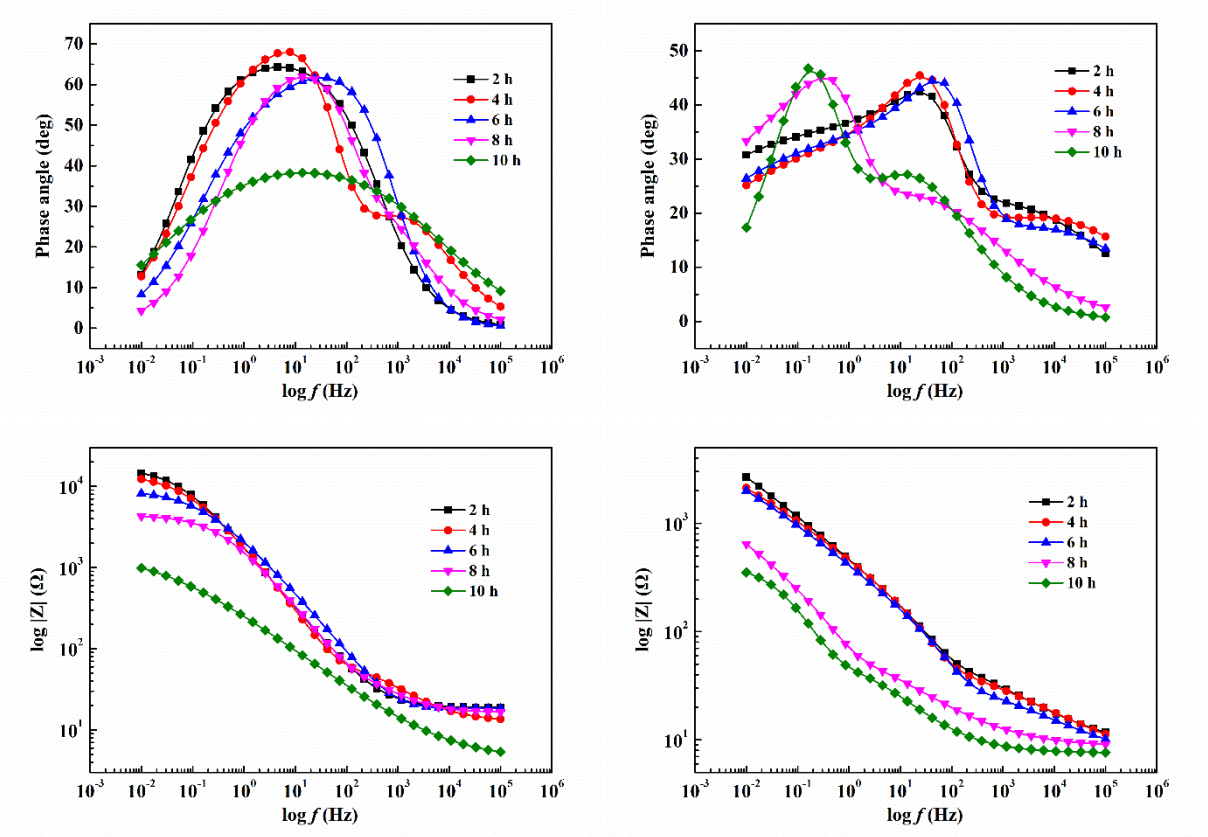

(1) 50℃ (-1.09 V) (2) 80℃ (-1.27 V)

Figure 6. The EIS curves of 1# sample (HRB335 steel) at different immersing time in 3 wt % NaCl solution of 2-10 h under different temperatures (t = 50℃ and 80℃) and CP potential (CP = -1.09 V and -1.27 V): (1) t = 50℃ and CP = -1.09 V, and (2) t = 80℃ and CP = -1.27 V

Table 3. The fitting parameters of EIS curves of 1# sample (HRB335 steel) at different immersing time in 3 wt % NaCl solution of 2-10 h under different temperatures (t = 50℃ and 80℃) and CP potential (CP = -1.09 V and -1.27 V)

Temperature	Parameter / Time	R_s ($\Omega\cdot cm^2$)	Q (F/cm^2)	n	R_p ($\Omega\cdot cm^2$)	C_{dl} (F/cm^2)	R_{ct} ($\Omega\cdot cm^2$)
50℃	2 h	1.88	1.37×10^{-4}	0.75	7.04×10^{1}	6.43×10^{-4}	1.43×10^{4}
	4 h	1.28	1.15×10^{-4}	0.65	6.80×10^{1}	2.86×10^{-5}	9.50×10^{3}
	6 h	1.82	1.19×10^{-4}	0.64	2.89×10^{1}	7.95×10^{-6}	9.10×10^{3}
	8 h	1.63	1.30×10^{-4}	0.70	7.21×10^{1}	1.09×10^{-4}	4.38×10^{3}
	10 h	4.36	1.48×10^{-3}	0.47	1.48×10^{1}	4.63×10^{-3}	1.33×10^{2}
80℃	2 h	7.77	9.88×10^{-4}	0.40	9.44×10^{1}	1.56×10^{-5}	1.62×10^{4}
	4 h	5.76	1.02×10^{-3}	0.38	6.28×10^{1}	2.35×10^{-5}	7.59×10^{3}
	6 h	5.97	1.54×10^{-3}	0.39	4.12×10^{1}	1.67×10^{-6}	7.74×10^{3}
	8 h	8.54	3.25×10^{-3}	0.44	9.57×10^{1}	1.19×10^{-3}	2.88×10^{3}

4. CONCLUSIONS

Based on immersion and electrochemical experiments, the optimal CP potential of reinforcement under different temperatures was studied through corrosion rate, corrosion morphology, electrochemical parameters, and the electrochemical characteristics of the metal at the opening under the condition of optimal CP potential. The conclusions drawn from the study are as follows.

(1) With the increase of cathodic protection potential, the general corrosion rate and pitting corrosion rate of HRB335 steel remain unchanged at 20℃, showing a general corrosion state. In contrast, at 50℃ and 80℃, the general corrosion rate and pitting rate decrease gradually, and the corrosion morphology changed from pitting to general corrosion. The polarization curves under different temperatures indicated that the oxygen diffusion process controlled the optimal CP potential. Considering the corrosion rate, morphology, and electrochemical reaction control process, the optimal CP potential was -1.0 V at 50℃ and -1.1 V at 80℃.

(2) In the crevice structure, when the HRB335 steel in the deepest crevice reaches the optimal CP potential, the metal in the opening may be in the over-protected state, and hydrogen evolution reaction occurred. The higher the temperature, the higher was the metal potential, and the more pronounced was the hydrogen evolution reaction.

References

1. L. Yan, G.L. Song, Z.M. Wang and D.J. Zheng, *Constr. Build. Mater.*, 296 (2021) 123587.
2. Y.Z. Mao, Y.H. Wei, H.T. Zhao, C.X. Lv, H.J. Cao and J. Li, Acta Metall. Sin-Engl., 31 (2018) 1171.
3. J. Shen, G. Song, D. Zheng and Z. Wang, *Mater. Corros*., 70 (2019) 2228.
4. L. Bertolini, F. Bolzoni, P. Pedeferri, L. Lazzari and T. Pastore, *J. Appl. Electrochem.*, 28 (1998) 1321.
5. F.M.Al. Mutlaq and C.L. Page, *Constr. Build. Mater.*, 39 (2013) 60.
6. W. Vélez, F. Matta and P. Ziehl, *Mater. Struct.*, 49 (2016) 507.
7. G.T. Parthiban, T. Parthiban, R. Ravi, V. Saraswathy, N. Palaniswamy and V. Sivan, *Corros. Sci.*, 50 (2008) 3329.
8. D.K. Kamde and R.G. Pillai, *Constr. Build. Mater.*, 237 (2020) 117616.
9. B. Leporace-Guimil, A. Conforti, R. Zerbino and G.A. Plizzari, *Cement Concrete Comp.*, 124 (2021) 104245.
10. A.M. Aguirre-Guerrero, R.A. Robayo-Salazar and R.M. de Gutiérrez, *J. Build. Eng.*, 33 (2021) 101593.
11. G.S. Steeb and R. Tank, *Mater. Corros.*, 60 (2015) 344.
12. G.T. Parthiban, T. Parthiban, R. Ravi, V. Saraswathy, N. Palaniswamy and V. Sivan, *Corros. Sci.*, 50 (2008) 3329.
13. Rasheeduzzafar, M.G. Ali and G.J. Al-Sulaimani, *Aci Mater. J.*, 90 (1993) 8.
14. E. Redaelli and L. Bertolini, *J. Appl. Electrochem.*, 41 (2011) 829.
15. E. Redaelli, F. Lollini and L. Bertolini, *Constr. Build. Mater.*, 39 (2013) 95.
16. O. Chaix, H.W. Hartt and R. Kessler, *Corrosion*, 51 (1995) 386.
17. W.H.A. Peelen, R.B. Polder, E. Redaelli and L. Bertolini, *Mater. Corros.*, 59 (2008) 81.
18. K. Ishii, H. Seki and T. Fukute, *Constr. Build. Mater.*, 12 (1998) 125.
19. M.G. Ali, Rasheeduzzafar and S.S. Al-Saadoun, *Cement Concrete Res.*, 22 (1992) 79.

20. J. García, F. Almeraya, C. Barrios, C. Gaona, R. Núnez, I. Lopez, M. Rodriguez, A. Martinez-Villafaee and J.M. Bastidas, *Cement Concrete Comp.*, 34 (2012) 242.
21. R.B. Polder, G. Leegwater, D. Worm and W. Courage, *Cement Concrete Comp.*, 47 (2014) 69.
22. H.M. Oleiwi, W. Yu, M. Curioni, X. Chen and I.L. Shabalin, *Mater. Struct.*,51 (2018) 148.
23. K. Wilson, M. Jawed and V. Ngala, *Constr. Build. Mater.*, 39 (2013) 19.
24. L. Bertolini, P. Pedeferri, E. Redaelli and T, *Mater. Corros.*, 54 (2003) 163.
25. A. Goyal, H.S. Pouya and E. Ganjian, *Constr. Build. Mater.*, 223 (2019) 1083.
26. K. Takewaka, *Corros. Sci.*, 35 (1993) 1617.
27. Z.L. Li, C. Yang, G. Cui, S.X. Zhang amd Chengbin Zhang, *Anti-Corros. Method. M.*, 66 (2019) 203.
28. R.D. Moser, P.M. Singh, L.F. Kahn, K.E. Kurtis, D.G. Nino and Z.B. Mcclelland, *Constr. Build. Mater.*, 203 (2019) 366.